Electrostatic recognition and induced fit in the k-PVIIA toxin binding to Shaker potassium channel

ARTICLE *in* JOURNAL OF THE AMERICAN CHEMICAL SOCIETY · JUNE 2005

Impact Factor: 12.11 · DOI: 10.1021/ja042641q · Source: PubMed

3 AUTHORS, INCLUDING:

Huan-Xiang Zhou
Florida State University
259 PUBLICATIONS **10,163** CITATIONS

J|A|C|S
ARTICLES
Published on Web 04/16/2005

Electrostatic Recognition and Induced Fit in the κ-PVIIA Toxin Binding to *Shaker* Potassium Channel

Xiaoqin Huang,[†] Feng Dong,[‡] and Huan-Xiang Zhou*[,†,§]

Contribution from the Institute of Molecular Biophysics and School of Computational Science, Department of Physics, Florida State University, Tallahassee, FL32306, and Department of Physics, Drexel University, Philadelphia, Pennsylvania 19104

Received December 7, 2004; E-mail: zhou@sb.fsu.edu

Abstract: Brownian dynamics (BD) and molecular dynamics (MD) simulations and electrostatic calculations were performed to study the binding process of κ-PVIIA to the *Shaker* potassium channel and the structure of the resulting complex. BD simulations, guided by electrostatic interactions, led to an initial alignment between the toxin and the channel protein. MD simulations were then carried out to allow for rearrangements from this initial structure. After ~4 ns, a critical "induced fit" process was observed to last for ~2 ns. In this process, the interface was reorganized, and side chains were moved so that favorable atomic contacts were formed or strengthened, while unfavorable contacts were eliminated. The final complex structure was stabilized through electrostatic interactions with the positively charged side chain of Lys7 of κ-PVIIA deeply inserted into the channel pore and other hydrogen bonds and by hydrophobic interactions involving Phe9 and Phe23 of the toxin. The validity of the predicted structure for the complex was assessed by calculating the effects of mutating charged and polar residues of both the toxin and the channel protein, with the calculated effects correlating reasonably well with experimental data. The present study suggests a general binding mechanism, whereby proteins are pre-aligned in their diffusional encounter by long-range electrostatic attraction, and nanosecond-scale rearrangements within the initial complex then lead to a specifically bound complex.

Introduction

Electrostatic recognition provides a mechanism for the fast binding of peptides and proteins to their targets.[1−11] The initial approach of a ligand to its target can be accelerated by the long-range electrostatic attraction. Once near the binding site, short-range interactions such as hydrophobic contacts and hydrogen bonding come into play; reorientation and conformational adjustments then take place to achieve multiple specific interactions, leading to a specific structure for the complex. For example, a 240-fold rate enhancement for the substrate binding to acetylcholinesterase was attributed to the electrostatic attraction around the active site.[2] Similar effects by surface charged residues were also observed for the binding of fasciculin to acetylcholinesterase.[3,4] Another prototypical case is the binding of barnase to barstar.[5−9,11] As shown in our previous studies, the binding rate for these two proteins is enhanced by long-range electrostatic attractions, and the final complex is stabilized by interfacial charge−charge interactions.[7,8,11] It has been observed experimentally that the affinities for the binding of snail toxins to nicotinic acetylcholine receptors can be substantially reduced by charge reversal mutations.[12,13] The κ-PVIIA toxin, with positively charged residues on the surface,[14,15] can bind very fast (with $k_{on} \approx 10^7-10^8$ $M^{-1}s^{-1}$)[16−19] with the *Shaker* potassium channel, which is rich in negatively charged residues on the extracellular side.[20−26] This system provides a good

[†] Institute of Molecular Biophysics and School of Computational Science, Florida State University.
[§] Department of Physics, Florida State University.
[‡] Department of Physics, Drexel University.

(1) Zhou, H.-X. *Biophys. J.* **1993**, *59*, 427−433.
(2) Zhou, H.-X.; Briggs, J. M.; McCammon, J. A. *J. Am. Chem. Soc.* **1996**, *118*, 13069−13070.
(3) Radic, Z.; Kirchhoff, P.; Quinn, D. M.; McCammon, J. A.; Taylor, P. *J. Biol. Chem.* **1997**, *272*, 23265−23277.
(4) Elcock, A. H.; Gabdoulline, R. F.; Wade, R. C.; McCammon, J. A. *J. Mol. Biol.* **1999**, *291*, 149−162.
(5) Schreiber, G.; Fersht, A. R. *J. Mol. Biol.* **1995**, *248*, 478−486.
(6) Schreiber, G.; Fersht, A. R. *Nat. Struct. Biol.* **1996**, *3*, 427−431.
(7) Vijayakumar, M.; Wong, K.-Y.; Schreiber, G.; Fersht, A. R.; Szabo, A.; Zhou, H.-X. *J. Mol. Biol.* **1998**, *278*, 1015−1024.
(8) Zhou, H.-X. *Biopolymers* **2001**, *59*, 427−433.
(9) Gabdoulline, R. F.; Wade, R. C. *J. Mol. Biol.* **2001**, *306*, 1139−1155.
(10) Zhou, H.-X. *J. Phys. Chem. B* **2002**, *106*, 2393−2397.
(11) Dong, F.; Vijayakumar, M.; Zhou, H.-X. *Biophys. J.* **2003**, *85*, 49−60.
(12) Osaka, H.; Malany, S.; Molles, B. E.; Sine, S. M.; Tayor, P. *J. Biol. Chem.* **2000**, *275*, 5478−5484.
(13) Papineni, R. V. L.; Sanchez, U. S.; Baksi, K.; Wilcockson, I. U.; Pedersen, S. E. *J. Biol. Chem.* **2001**, *276*, 23589−23598.
(14) Scanlon, M. J.; Naranjo, D.; Thomas, L.; Alewood, P. F.; Lewis, R. J.; Craik, D. J. *Structure* **1997**, *5*, 1585−1597.
(15) Savarin, P.; Guenneugues, M.; Gilquin, B.; Lamthanh, H.; Gasparini, S.; Zinn-Justin, S.; Menez, A. *Biochemistry* **1998**, *37*, 5407−5416.
(16) Garcia, E.; Scanlon, M.; Nanrojo, D. *J. Gen. Physiol.* **1999**, *114*, 141−157.
(17) Terlau, H.; Boccaccio, A.; Olivera, B. M.; Conti, F. *J. Gen. Physiol.* **1999**, *114*, 125−140.
(18) Naranjo, D. *Biophys. J.* **2002**, *82*, 3003−3011.
(19) Koch, E. D.; Oliveray, B. M.; Terlau, H.; Contiz, F. *Biophys. J.* **2004**, *86*, 191−209.
(20) Gross, A.; MacKinnon, R. *Neuron* **1996**, *16*, 399−406.
(21) Ranganathan, R.; Lewis, J. H.; MacKinnon, R. *Neuron* **1996**, *16*, 131−139.
(22) Kreusch, A.; Pfaffinger, P. J.; Stevens, C. F.; Choe, S. *Nature* **1998**, *392*, 945−948.
(23) Jacobsen, R. B.; Koch, E. D.; Lange-Maleck, B.; Stocker, M.; Verhey, J.; Wagoner, R. M. V.; Vyazovkina, V.; Oliveray, B. M.; Terlau, H. *J. Biol Chem.* **2000**, *275*, 24639−24644.

10.1021/ja042641q CCC: $30.25

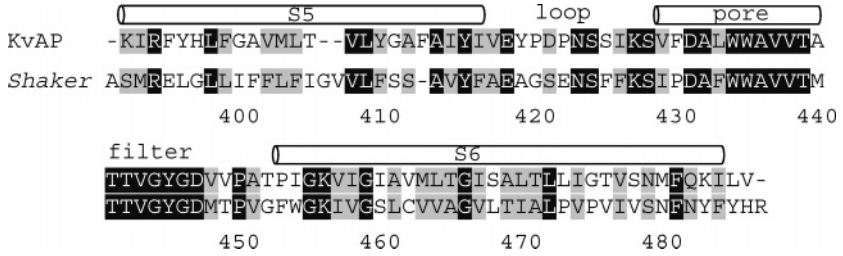

Figure 1. Sequence alignment of the *Shaker* K^+ channel with KvAP. Dark shaded letters show identical residues, whereas light shaded letters show conservative substitutions. Helices of KvAP (PDB entry 1orq) are indicated. *Shaker* residue numbering is given below the sequence.

paradigm for investigating the roles of electrostatic recognition and conformational rearrangements in the binding process. In this article we report our study of their binding by several complementary computational approaches including Brownian dynamics (BD) and molecular dynamics (MD) simulations. The insight gained on electrostatic recognition and induced fit appears to have implications for peptide/protein−protein binding in general.

The *Shaker* channel of the fruit fly *Drosphilia melanogaster* is one of the most extensively studied voltage-gated K^+ (Kv) channels.[20−31] It has the same structural architecture as other Kv channels, as revealed by electron microscopy.[25,26] This distinct two-layer architecture, formed by four identical subunits with C_4 symmetry, consists of a transmembrane (TM) and a cytoplasmic domain. In the TM domain, each subunit consists of six TM helices (named S1 to S6), of which S5 and S6 form the central conducting pore and are surrounded by the S1−S4 helices. Sequence alignment reveals a homology of 62% to the KcsA channel[32−34] and 68% to the KvAP channel[35] in the S5−S6 region (see Figure 1). This region contains the unique TTVGYG sequence serving as the K^+-selective filter and is the most conserved among Kv channels. Within S5−S6, the most variable segment is the loop between the S5 and pore helices, which is functionally implicated in the susceptibility to toxin binding.[20,21,24,36−39] Comparing all the available X-ray structures of Kv channels,[32−35,40−42] C_α root-mean-square deviations (RMSD) <2.0 Å are obtained for the S5 and S6 helices above the central cavity, the pore helix, and the selectivity filter, and the C_α RMSD is <0.5 Å for the selectivity filter alone. Functionally, the *Shaker* K^+ channel is also similar to other Kv channels, i.e. it regulates the flux of K^+ by opening and closing very quickly in response to changes in the potential difference across the membrane, and undergoes a conformational rearrangement in this process.[30,31,36−38] The sequence, structural, and functional similarities between the *Shaker* channel and other Kv channels and the existing crystal structures allow for the development of a homology model for the S5−S6 region of the *Shaker* channel, which forms the basis of the present study of its binding with κ-PVIIA.

κ-PVIIA, derived from the venom of *Conus purpurascens*, is the first member of a new family of conotoxins.[16,17] Its amino acid sequence and three-dimensional structure bear little apparent similarity with other toxins such as dendrotoxins or scorpion toxins.[14,15,43] A single κ-PVIIA molecule can bind to a single *Shaker* K^+ channel in both the open and closed states with similar molecular interactions, but with a somewhat higher binding affinity ($K_d \approx 50$ nM) for the closed state channel.[16−19,23] On the basis of NMR structures for the toxin, two possible modes have been proposed for the binding of κ-PVIIA to the *Shaker* channel. In one (denoted as mode I in future reference), Lys7 of the toxin was proposed to be positioned into the vestibule of the channel.[15] In the other (mode II), Lys19 of the toxin was suggested to physically occludes the pore of the channel.[14] A site-directed mutagenesis study has indicated key residues for binding that appear to be more in line with mode I.[23]

Ultimately a detailed understanding of the channel blockage by κ-PVIIA requires an atomic structure for the channel−toxin complex. Is it possible to theoretically distinguish the two proposed modes of binding? What conformational changes, if any, will the toxin undergo before forming a specific complex? Are there general mechanistic principles to be extracted from the study of κ-PVIIA binding to the *Shaker* channel? These questions motivated the present study. We used BD simulations of the toxin to select for binding configurations that are consistent with either of the two proposed modes. The electrostatic energy of interaction with the channel protein strongly favored binding mode I. We then investigated structural reorganizations within such a pre-aligned complex by MD simulations. Through a 13.2-ns trajectory, a specific complex was obtained. In this complex, Lys7 of κ-PVIIA was inserted into the channel pore, and numerous hydrogen bonds and hydrophobic interactions (involving Phe9 and Phe23 of the toxin) were also formed. This predicted complex structure was

(24) Shealy, R. T.; Murphy, A. D.; Ramarathnam, R.; Jakobsson, E. *Biophys. J.* **2003**, *84*, 2929−2942.
(25) Sokolova, O.; Accardi, A.; Gutierrez, D.; Lau, A.; Rigney, M.; Grigorieff, N. *Proc. Natl. Acad. Sci. U.S.A.* **2003**, *100*, 12607−12612.
(26) Sokolova, O. *FEBS Lett.* **2004**, *564*, 251−256.
(27) Shon, K.-J.; Stocker, M.; Terlau, H.; Stuhmer, W.; Jacobsen, R.; Walker, C.; Grilley, M.; Watkinsi, M.; Hillyardi, D. R.; Gray, W. R.; Olivera, B. M. *J. Biol. Chem.* **1998**, *273*, 33−38.
(28) Ranatunga, K. M.; Law, R. J.; Smith, G. R.; Sansom, M. S. P. *Eur. Biophys. J.* **2001**, *30*, 295−303.
(29) Eriksson, M. A. L.; Roux, B. *Biophys. J.* **2002**, *83*, 2595−2609.
(30) MacKinnon, R.; Aldrich, R.; Lee, A. W. *Science* **1993**, *262*, 757−759.
(31) Sigg, D.; Bezanilla, F.; Stefani, E. *Proc. Natl. Acad. Sci. U.S.A.* **2003**, *100*, 76111−77615.
(32) Doyle, D. A.; Cabral, J. M.; Pfuetzner, R. A.; Kuo, A.; Gulbis, J. M.; Cohen, S. L.; Chait, B. T.; MacKinnon, R. *Science* **1998**, *280*, 69−76.
(33) Zhou, M.; Morais-Cabral, J. H.; Mann, S.; MacKinnon, R. *Nature* **2001**, *411*, 657−660.
(34) Zhou, Y.; Morals-Cabral, J. H.; Kaufman, A.; MacKinnon, R. *Nature* **2001**, *414*, 43−48.
(35) Jiang, Y.; Lee, A.; Chen, J.; Ruta, V.; Cadene, M.; Chalt, B. T.; MacKinnon, R. *Nature* **2003**, *423*, 33−41.
(36) MacKinnon, R.; Cohen, S. L.; Kuo, A.; Lee, A.; Chait, B. T. *Science* **1998**, *280*, 106−109.
(37) Perozo, E.; Cortes, D. M.; Cuello, L. G. *Science* **1999**, *285*, 73−77.
(38) Lu, Z.; Klem, A. M.; Ramu, Y. *Nature* **2001**, *413*, 809−813.
(39) MacKinnon, R. *FEBS Lett.* **2003**, *555*, 62−65.
(40) Jiang, Y.; Lee, A.; Chen, J.; Cadene, M.; Chait, B. T.; MacKinnon, R. *Nature* **2002**, *417*, 515−522.
(41) Jiang, Y.; Lee, A.; Chen, J.; Cadene, M.; Chait, B. T.; MacKinnon, R. *Nature* **2002**, *417*, 523−526.
(42) Kuo, A.; Gulbis, J. M.; Antcliff, J. F.; Rahman, T.; Lowe, E. D.; Zimmer, J.; Cuthbertson, J.; Ashcroft, F. M.; Ezaki, T.; Doyle, D. A. *Science* **2003**, *300*, 1922−1926.
(43) Rodriguez de la Vega, R. C.; Merino, E.; Becerril, B.; Possani, L. D. *Trends Pharmacol. Sci.* **2003**, *24*, 222−227.

validated by reasonable correlation with site-directed mutagenesis data.

Computational Methods

Homology Model of the *Shaker* Channel Pore. A homology model for the *Shaker* channel, from the beginning of S5 to the end of S6 (amino acids 391−487), was built on the crystal structure of the corresponding region of KvAP (PDB entry 1orq at 3.2 Å resolution)[35] with InsightII (version 2000, Accelrys, San Diego, CA). The sequence alignment, shown in Figure 1, was generated by ClusterW[44] with the Blosum scoring function.[45] Backbone positions and conserved side-chain positions were directly transformed from the template structure, while positions for nonconserved side chains were built and relaxed within the homology module of InsightII. Two residues, G406 and V407, were inserted by extending the S5 helix toward the intracellular side while keeping the helix orientation (see sequence alignment in Figure 1). The homotetrameric pore structure was constructed by preserving the C_4 symmetry. Two K^+ ions were inserted, one at site 3 (between the carbonyls of Thr442 and Val443) and the other at the central cavity. In addition, a water molecule was placed at site 2 (between the carbonyls of Val443 and Gly444). Finally the modeled structure was energy minimized by the conjugate-gradient algorithm using the CHARMM27 force field.[46] The net charge on the homotetramer is $-4e$ at pH 7.

BD Simulations. κ-PVIIA contains 27 residues, with three disulfide bonds (Cys1 to Cys16, Cys8 to Cys20, and Cys15 to Cys26) and a net charge of $+4e$ at pH 7.[14,15] The two sets of NMR structures, with 22 models determined by Savarin et al.[15] (PDB entry 1kcp) and 20 models determined by Scanlon et al.[14] (PDB entry 1av3), were quite similar. BD simulations were used to distinguish the two proposed modes of binding and obtain an initial alignment for κ-PVIIA with respect to the *Shaker* channel. For this purpose, the channel protein was treated as an immobile target located at the origin, and BD trajectories of κ-PVIIA were launched from a spherical surface at a radius of 70 Å.[3,4] The trajectories were terminated either when the distance to the channel reached 200 Å or a "reaction" criterion was satisfied. This criterion was based on the distance between the NZ atom of either Lys7 or Lys19 of the toxin and the K^+ ion at site 3 in the channel and was satisfied when the distance fell below 20 Å. That cutoff distance was chosen on the basis of the following considerations. The distance from site 3 to the pore entrance is $\sim$ 10 Å. The additional 10 Å provided room for adequately sampling of configurations satisfying the reaction criterion and yet was sufficiently short such that the sampled configurations had electrostatically favorable orientations. 1kcp models (22 NMR conformations) were used in conjunction with the Lys7 criterion, while 1av3 (20 NMR conformations) models were used in conjunction with the Lys19 criterion. For each model, 5000 trajectories were launched. The final configurations satisfying the distance criterion were recorded for later analysis. The term "configuration" specifically refers to the relative orientation and positioning of the toxin and the channel within a complex.

BD simulations were carried out by the MacroDox program,[47] in which electrostatic interactions were treated by the test-charge model. The electrostatic potential of the channel protein was calculated once, and multiplication with the charges on the toxin gave the interaction energy. Although the test-charge model was shown to be deficient as it fails to treat the low dielectric inside the toxin,[1,9] the high calculation speed justified its usage for the limited purpose of identifying the initial alignment of the toxin with respect to the channel protein. Other studies[48,49] have shown that the test-charge model could be used to identify a reasonable initial complex of two proteins.

MD Simulations. Once the toxin and the channel come into contact, they will undergo conformational rearrangements to reach a stably bound state. These rearrangements were investigated by MD simulations. The S5−S6 region of the *Shaker* channel was situated in a bilayer of 124 POPC lipid molecules[50] at a position derived from available X-ray structures,[32−35] with the outer ring of Trp residues aligned with the polar headgroups of the lipids. κ-PVIIA was then introduced to the pre-aligned configuration selected from the BD simulations. The channel−toxin complex and the associated lipid bilayer (to be collectively called the solute in future reference) were solvated by 19,908 water molecules, and two Cl^- ions were added in the solvent to make the system electrically neutral. The whole system contained a total of 72,700 atoms (see Figure 2), and the simulation box had an initial size of $99 \times 99 \times 105$ Å^3.

The MD simulations were performed on an IBM SP4 supercomputer by using the SANDER module in AMBER7.0.[51] The water model was TIP3P.[52,53] To start off, the solute and then the solvent were each subjected to conjugate-gradient energy minimizations of 1000 steps. To avoid possible aggregation of vacuum bubbles and small gaps at the edges of the box due to solvent packing, a 5-ps MD equilibration at constant volume was performed. After that, the solute and solvent were energy minimized again using the same cycles as before, followed by 1000 steps of minimization for the whole system. The whole system was then gradually heated to 300 K and equilibrated for 200 ps. Finally the MD trajectory was run at constant temperature and constant pressure for a total time of 13.2 ns. In the last 7.2 ns no significant conformational adjustments were seen, and hence, the simulations were not continued. The entire simulations took about 3 months. Throughout the simulations, a 9-Å nonbonded interaction cutoff was used, and the nonbonded list was updated once every 100 steps. The particle mesh Ewald method[54−57] was applied to treat electrostatic interactions. The lengths of bonds involving hydrogen atoms were fixed with the SHAKE algorithm,[58] enabling the use of a 2-fs time step to integrate the equations of motion. The system was coupled to a thermal bath at 300 K by the weak-coupling method.[59,60] After each picosecond the solute center of mass motion was removed to avoid the "cold solute/hot solvent" problem.

Calculations on the Effects of Charge and Polar Mutations. In the last 7.2 ns of the MD trajectory, a specific complex between κ-PVIIA and the *Shaker* channel was formed. The validity of this complex was assessed by comparing key residues in the interface against those identified by experiments.[19,23,27] In addition, we also calculated the effects of mutations on binding affinity to see whether this complex allowed for quantitative correlation with experimental data.

(44) Thompson, J. D.; Higgins, D. G.; Gibson, T. J. *Nucleic Acids Res.* **1994**, *22*, 4673−4680.
(45) Henikoff, S.; Henikoff, J. G. *Proc. Natl. Acad. Sci. U.S.A.* **1992**, *89*, 10915−10919.
(46) Brooks, B. R.; Bruccoleri, R. E.; Olafson, B. D.; States, D. J.; Swaminathan, S.; Karplus, M. *J. Comput. Chem.* **1983**, *4*, 187−217.
(47) Northrup, S. H.; Laughner, T.; Stevenson, G. Tennessee Technological University: Cookeville, TN, 1999.
(48) Cui, M.; Shen, J.; Briggs, J. M.; Fu, W.; Wu, J.; Zhang, Y.; Luo, X.; Chi, Z.; Ji, R.; Jiang, H.; Chen, K. *J. Mol. Biol.* **2002**, *318*, 417−428.
(49) Fu, W.; Cui, M.; Briggs, J. M.; Huang, X.; Xiong, B.; Zhang, Y.; Luo, X.; Shen, J.; Ji, R.; Jiang, H.; Chen, K. *Biophys. J.* **2002**, *83*, 2370−2385.
(50) Lin, J. H.; Baker, N. A.; McCammon, J. A. *Biophys. J.* **2002**, *83*, 1374−1379.
(51) Case, D. A.; Pearlman, D. A.; Caldwell, J. W.; Cheatham, T. E., III; Wang, J.; Ross, W. S.; Simmerling, C. L.; Darden, T. A.; Merz, K. M.; Stanton, R. V.; Cheng, A. L.; Vincent, J. J.; Crowley, M.; Tsui, V.; Gohlke, H.; Radmer, R. J.; Duan, Y.; Pitera, J.; Massova, I.; Seibel, G. L.; Singh, U. C.; Weiner, P. K.; Kollman, P. A. University of California: San Francisco, CA, 2002.
(52) Jorgensen, W. L.; Chandrasekhar, J.; Madura, J. D.; Impey, R. W.; Klein, M. L. *J. Chem. Phys.* **1983**, *79*, 926−935.
(53) Neria, E.; Fisher, S.; Karplus, M. *J. Chem. Phys.* **1996**, *105*, 1902−1921.
(54) Darden, T.; York, D.; Pedersen, L. *J. Chem. Phys.* **1993**, *98*, 10089−10092.
(55) Essmann, U.; Perera, L.; Berkowitz, M. L.; Darden, T.; Lee, H.; Pedersen, L. G. *J. Chem. Phys.* **1995**, *103*, 8577−8593.
(56) Sagui, C.; Darden, T. A. *Annu. Rev. Biophys. Biomol. Struct.* **1999**, *28*, 155−179.
(57) Toukmaji, A.; Sagui, C.; Board, J.; Darden, T. *J. Chem. Phys.* **2000**, *113*, 10913−10927.
(58) Ryckaert, J. P.; Ciccotti, G.; Berendsen, H. J. C. *J. Comput. Phys.* **1997**, *23*, 327−341.
(59) Berendsen, H. J. C.; Postma, J. P. M.; van Gunsteren, W. F.; DiNola, A.; Haak, J. R. *J. Chem. Phys.* **1984**, *81*, 3684−3690.
(60) Morishita, T. *J. Chem. Phys.* **2000**, *113*, 2976−2982.

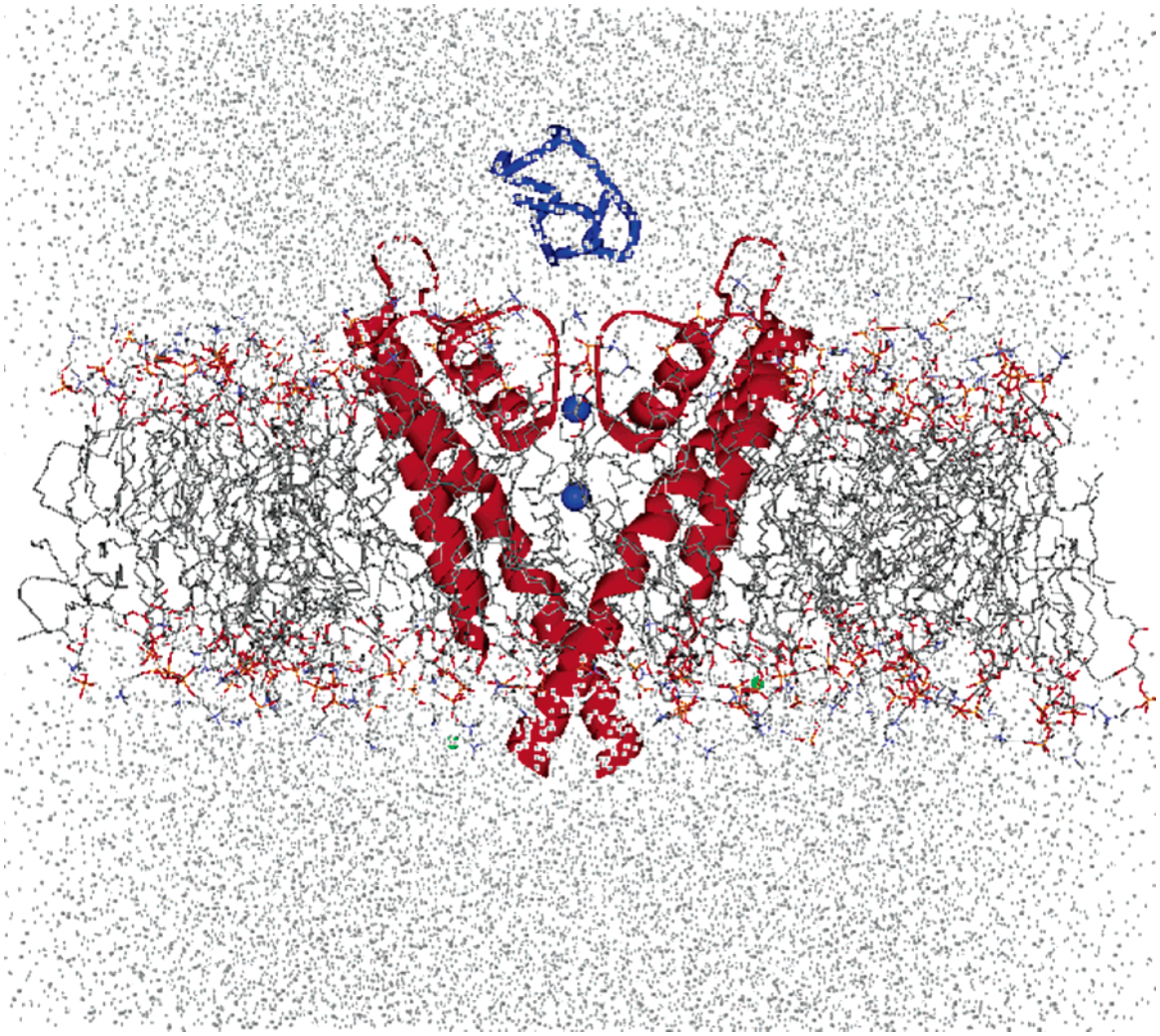

Figure 2. Side view of the unit cell of the MD simulations. For clarity, only two subunits of the *Shaker* K^+ channel are presented as red ribbons. κ-PVIIA toxin is shown as a blue tube. Two K^+ ions in the channel pore are shown as blue spheres, and two Cl^- counterions are shown as green spheres. POPC lipid molecules appear as sticks, and water molecules as gray dots.

For the electrostatic calculations, a procedure established in our previous studies[7,11,61−63] on the electrostatic contributions to protein folding stability and binding stability and rate was adapted. Briefly, 21 conformations for the κ-PVIIA−*Shaker* complex were sampled from the last 7.2 ns of the MD trajectory. Point mutations were generated in InsightII, and newly created side chains were optimized by energy minimizing using the CHARMM force field.[46] For the channel, each point mutation involved modeling all four identical positions within the tetramer. After assigning Amber charges (at pH 7) and radii[51] to the complex, the Poisson−Boltzmann equation was solved by the UHBD program.[64] The dielectric boundary was taken to be the outer van der Waals surface of the complex, with dielectric constants set to 4 and 78, respectively, for the complex and the solvent. Any voids inside the outer van der Waals surface were assigned the low dielectric constant. The ionic strength was 0.1 M (with a 2-Å ion exclusion radius), and temperature was 298 K. The electrostatic potential ϕ was calculated first on a 100 × 100 × 100 grid with 1.5 Å spacing centered at the geometric center of the complex, then followed by a 180 × 180 × 180 grid with 0.7 Å spacing at the same center. A final round of focusing at the backbone nitrogen atom of a mutation site was introduced on a 200 × 200 × 200 grid with 0.25 Å spacing. The electrostatic free energy of the protein complex (AB) was calculated as

$$G_{el}^{AB} = \frac{1}{2}\sum_{i=1}^{N} q_i \phi_i \qquad (1)$$

where q_i are the partial charges and N is the total number of atoms of the complex. The same procedure was followed in calculating the electrostatic energy of each subunit (A or B), except that the other subunit (B or A) was stripped away. The electrostatic contribution to the binding affinity was calculated as

$$\Delta G_{el} = G_{el}^{AB} - G_{el}^{A} - G_{el}^{B} \qquad (2)$$

The electrostatic contribution of each mutation to the binding stability of the complex was taken as $\Delta\Delta G_{el}$, the difference in ΔG_{el} between the mutant and the wild type, averaged over the 21 conformations. Inclusion of the lipids as a part of the *Shaker* channel did not change the calculation results significantly. Effects for a total of 8 mutations on κ-PVIIA and 16 mutations on the *Shaker* channel were calculated and compared with experimental mutagenesis data.[23]

Results

Electrostatic Potentials. In previous studies, we quantitatively rationalized electrostatic enhancement of protein associa-

(61) Vijayakumar, M.; Zhou, H.-X. *J. Phys. Chem. B* **2001**, *105*, 7334−7340.
(62) Dong, F.; Zhou, H.-X. *Biophys. J.* **2002**, *83*, 1341−1347.
(63) Zhou, H.-X.; Dong, F. *Biophys. J.* **2003**, *84*, 2216−2222.
(64) Madura, J. D.; Briggs, J. M.; Wade, R. C.; Davis, M. E.; Luty, B. A.; Ilin, A.; Antosiewicz, J.; Gilson, M. K.; Bagheri, B.; Scott, L. R.; Mccammon, J. A. *Comput. Phys. Commun.* **1995**, *91*, 57−95.

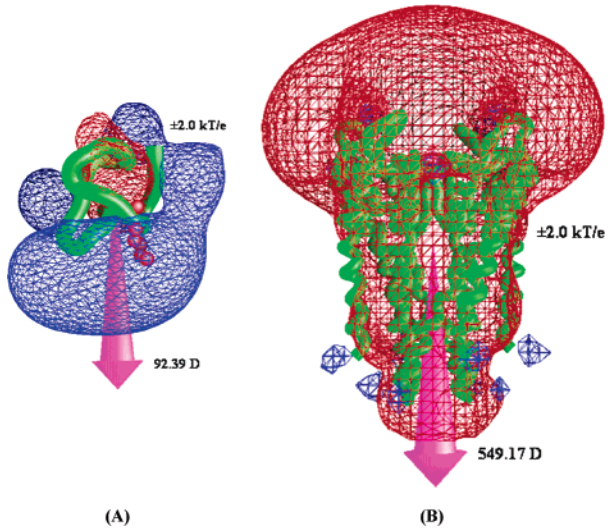

Figure 3. Electrostatic potential contour maps for the κ-PVIIA toxin and the *Shaker* K^+ channel. Isopotential surfaces at $\pm 2k_BT/e$ are shown in blue and red, respectively. Arrows indicate the directions of the dipoles of the toxin and channel.

tion rate and electrostatic contributions to protein binding stability by individual residues.[1,7,8,10,11] One of the conclusions was that long-range electrostatic attraction can significantly increase the association rate between two proteins by lowering the free energy of the transition state for association. Similar conclusions were reached in other studies on the role of electrostatic interactions in protein association.[3−6,9] In the case of κ-PVIIA binding to the *Shaker* K^+ channel, a similar role of long-range electrostatic attraction can be assigned from a calculation of the electrostatic potentials of the toxin and the channel protein. As shown in Figure 3, the κ-PVIIA surface has a large positive potential that could be correlated with the distribution of positive charged residues in its sequence. The pore structure of the *Shaker* channel, on the other hand, bears a large negative electrostatic potential, which is symmetric around the central axis. The complementary potential surfaces of κ-PVIIA and the *Shaker* channel strongly suggest that electrostatic attraction will help the approach of the toxin to the channel. Results from BD simulations presented below indeed show that the long-range attraction led to the toxin's alignment with some of its Lys and Arg residues pointing toward the channel pore.

Selection of Pre-aligned Toxin Conformations by BD Simulations. For each NMR model of κ-PVIIA, the final configurations of BD trajectories that satisfied a distance-based reaction criterion were collected. The 1kcp set of 22 NMR models used a reaction distance calculated on the toxin Lys7 residue, selecting mode I binding. On the other hand, the 1av3 set of 20 NMR models used a reaction distance calculated on the toxin Lys19 residue, selecting mode II binding. BD configurations for each NMR model were clustered according to the orientations of the toxin with respect to the *Shaker* channel. Specifically, the three residue-based toxin−channel contacts with the shortest distances were identified, and configurations with the same contact triplets were collected in one cluster. For each NMR model, the cluster with the lowest average electrostatic interaction energy between the toxin and the channel was retained for further analysis. The numbers of configurations and the average electrostatic interaction energies of these clusters are listed in Table 1. As expected, clusters with lower interaction energies tended to be sampled more frequently by the BD simulations.

As mentioned earlier, mode I involves Lys7 of the toxin occluding the channel pore, whereas mode II involves Lys19. Despite this difference, the three *Shaker* residues forming shortest contacts with the toxin were almost identical among the 22 clusters of mode-I configurations and the 20 clusters of

Table 1. Contact Triplets and Electrostatic Interaction Energies Obtained from BD Simulations Using as Reaction Criteria Two Modes of Binding of κ-PVIIA to the *Shaker* K^+ Channel

mode I				mode II			
κ-PVIIA models	triplets	no.[a]	ΔG_{el} (kcal/mol)[b]	κ-PVIIA models	triplets	no.[a]	ΔG_{el} (kcal/mol)[b]
kcp1	447−2; 431−1; 427−13	86	−19.7	av1	447−19; 431−22; 427−18	125	−8.7
kcp2	447−7; 431−22; 427−2	157	−21.5	av2	447−19; 431−22; 427−25	319	−20.6
kcp3	447−25; 431−22; 427−1	45	−19.8	av3	447−19; 431−22; 427−25	145	−12.4
kcp4	447−22; 431−19; 427−19	1	−7.5	av4	447−19; 431−22; 427−25	92	−9.2
kcp5	447−25; 431−22; 427−2	191	−22.0	av5	447−19; 431−22; 427−18	89	−8.6
kcp6	447−7; 418−22; 427−2	184	−17.6	av6	447−19; 431−22; 427−25	93	−9.5
kcp7	447−7; 418−22; 427−2	175	−18.0	av7	447−19; 431−22; 427−18	98	−8.0
kcp8	447−2; 431−1; 427−14	78	−17.5	av8	447−19; 431−22; 427−25	96	−10.1
kcp9	447−7; 418−2; 427−14	120	−14.7	av9	447−19; 431−22; 427−25	179	−9.6
kcp10	447−25; 431−2; 418−22	212	−22.2	av10	447−19; 431−22; 427−25	85	−10.3
kcp11	447−7; 431−22; 427−2	28	−5.2	av11	447−19; 431−22; 427−25	89	−9.8
kcp12	447−7; 431−22; 427−19	142	−19.4	av12	447−19; 431−22; 427−25	51	−9.4
kcp13	447−25; 431−22; 427−2	141	−19.0	av13	447−19; 431−22; 427−25	73	−10.5
kcp14	447−25; 431−2; 427−1	68	−18.3	av14	447−19; 431−22; 427−25	66	−9.0
kcp15	447−25; 422−22; 427−2	76	−15.0	av15	447−19; 431−22; 427−18	113	−8.9
kcp16	447−7; 431−22; 418−22	601	−27.0	av16	447−19; 431−22; 427−25	83	−10.1
kcp17	447−7; 431−2; 427−14	581	−20.4	av17	447−19; 431−22; 427−18	86	−9.2
kcp18	447−7; 431−22; 427−2	323	−31.1	av18	447−19; 431−22; 427−25	75	−9.2
kcp19	447−7; 431−2; 427−1	168	−14.0	av19	447−19; 431−22; 427−25	100	9.6
kcp20	447−25; 431−2; 427−14	327	−22.4	av20	447−18; 431−22; 427−25	167	−14.2
kcp21	447−7; 431−2; 427−1	214	−20.4				
kcp22	447−7; 431−22; 427−2	324	−18.6				
average[c]		193	−18.7	average[c]		111	−9.4

[a] Number of configurations in the cluster with lowest averaged electrostatic interaction energy. [b] Lowest cluster average of electrostatic interaction energy. [c] Average over the NMR models of each binding mode.

mode-II configurations (the reader may find it useful here to refer to Figure 7, to be presented below). These were Asp447, Asp431, and Lys427. The identifications of Asp447 and Asp431 by the BD simulations are consistent with their roles suggested previously that the two rings of negative charges generate a field of electrostatic potential around the mouth of the *Shaker* pore and attract positively charged ligands.[28,32−35,39,65,66] Only in six clusters of mode-I configurations was Asp431 or Lys427 replaced either by Glu418 or Glu422. In all of the 20 mode-II configurations, the shortest contacts were formed by Asp447, Asp431, and Lys427, and their partners on the toxin were also nearly invariant: respectively they were Lys19, Arg22, and Lys25 or Arg18. In contrast, the contact partners in the mode-I configurations were much more variable. Most often the partner of Asp447 was toxin Lys7, but in 10 of the 22 clusters, the partner switched to Lys25, Arg2, or Arg22. The partner of Asp431 was distributed among Arg22, Arg2, the N-terminal residue, and Lys19, whereas the partner of Lys427 was distributed among Arg2, the N-terminal residue, Asp14, Asp13, and Lys19. The variability suggests that the *Shaker* channel exerts a stronger capture probability when the toxin is presented for mode I binding.

The two proposed modes of binding can be discriminated by the interaction energy or, equivalently, the number of configurations sampled. The data in Table 1 clearly shows that mode I led to much more favorable electrostatic interactions between κ-PVIIA and the *Shaker* channel. The 22 clusters of mode-I configurations had an average electrostatic interaction energy (−18.7 kcal/mol) that is twice in magnitude than the corresponding quantity (−9.4 kcal/mol) for the 20 clusters of mode-II configurations. The BD simulations thus suggest that mode I, with Lys7 positioned into the vestibule of the channel, is the preferred mode of toxin binding. This finding is in line with the site-directed mutagenesis study of Jacobsen et al.[23] showing that mutation of Lys7 led to a dramatic decrease on the IC_{50} value of κ-PVIIA, but mutation of Lys19 had a minimal effect.

Among the mode-I configurations, the cluster obtained from model 18 of the 1kcp set had the lowest average interaction energy (−31.1 kcal/mol). Within this cluster, the configuration with the lowest interaction energy (−35.4 kcal/mol) was selected as the pre-aligned starting complex for MD simulations.

To assess how representative this selection is, the 22 configurations with the lowest energies within the clusters of the 1kcp set were compared in relative orientations. Rotation matrixes between the model-18 configuration and all other 21 configurations were calculated. The results showed that, relative to the model-18 configuration, 5 configurations (from models 3, 12, and 14−16) had only slight rotations, 6 configurations (from models 7, 10, 13, 19, 20, and 22) were rotated by ∼180° around the axis along the central pore of the channel, and 8 configurations (from models 1, 2, 5, 6, 8, 9, 17, and 21) were rotated by ∼±90°. Since the *Shaker* channel has C_4 symmetry, each subunit is structurally identical, so the configurations with 180° and ±90° rotations are essentially the same as the model-18 configuration. With the exception of two configurations (from models 4 and 11) with much higher energies, all the 1kcp models resulted in the same pre-aligned complex, as represented by the model-18 configuration.

(65) Berneche, S.; Roux, B. *Nature* **2001**, *414*, 73−77.
(66) Domene, C.; Sansom, M. S. *Biophys. J.* **2003**, *85*, 2787−2800.

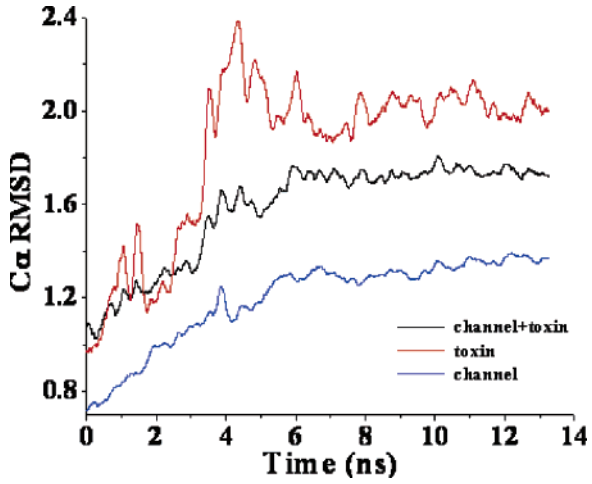

Figure 4. C_α RMSDs of κ-PVIIA, the *Shaker* channel, and their complex from the initial structure along the 13.2-ns MD trajectory.

Table 2. Residues Forming Stable Contacts during the Entire MD Trajectory

κ-PVIIA toxin			*Shaker* K⁺ channel		
residue	fraction[a]	contacts[b]	residue[c]	fraction[a]	contacts[b]
Arg2	1.00	11.8	Tyr445(A)	1.00	7.7
Cys8	0.98	13.8	Gly446(A)	1.00	14.0
Phe9	1.00	29.7	Asp447(A)	0.98	3.7
Gln10	0.99	20.6	Gly444(B)	0.75	0.8
Lys25	1.00	10.1	Tyr445(B)	1.00	6. 8
			Gly446(B)	1.00	13.1
			Val451(B)	0.74	0.9
			Tyr445(C)	1.00	5.1
			Tyr445(D)	1.00	6.1
			Gly446(D)	1.00	10.1

[a] Fraction of time in which at least one contact was formed during the MD simulations. [b] Average number of contacts over the entire trajectory. [c] Letters in parentheses indicate subunits.

MD Simulations of Induced Fit. Figure 4 presents the C_α RMSD from the starting structure (i.e., the model-18 configuration selected earlier) during the 13.2-ns production run of the MD simulations. The toxin showed much larger RMSD than the *Shaker* channel, indicating that κ-PVIIA is more flexible and experiences larger conformational changes in forming a specific complex. The toxin had especially high RMSD during the 4−6 ns period, suggesting induced-fit events. Afterward the RMSD of the toxin as well as the channel and the complex as a whole leveled off, suggesting that a specific complex had formed. The RMSD of the toxin, the channel and the complex during the last 7.2 ns fluctuated around 2.0, 1.3, and 1.7 Å, respectively.

To elucidate the details of the conformational and configurational changes in the first 6 ns, and to characterize the interactions that stabilize the complex, contacts between κ-PVIIA and the channel were calculated using an atomic distance cutoff of 5 Å. Contacts were collected at the residue level. Only residues that formed contacts more than 10% of the 13.2-ns trajectory were further analyzed, allowing for focusing on the important residues. These can be conveniently classified into four types: type-I residues formed stable contacts throughout the whole trajectory (Table 2); type-II residues experienced significant changes in contact formation during the 4−5 ns period; type-III residues experienced significant changes in contact formation during the 5−6 ns period; the remaining

Table 3. Residues Showing Changes in Contacts along the MD Trajectory

κ-PVIIA toxin			*Shaker* K+ channel		
residue	fraction[a]	feature[b]	residue	fraction[a]	feature[b]
Cys1	0.17	change in 4−5 ns	Asn423(B)	0.42	change in 4−5 ns
Ile3	0.36	random	Ser424(B)	0.76	random
Asn5	0.82	random	Phe425(B)	1.00	change in 4−5 ns
Gln6	0.49	random	Lys427(B)	0.68	random
Lys7	1.00	change in 4−5 ns	Asp447(B)	1.00	change in 5−6 ns
His11	0.86	random	Met448(B)	0.20	random
Leu12	1.00	change in 4−5 ns	Asn423(C)	0.88	random
Asp13	0.82	change in 4−5 ns	Ser424(C)	0.19	random
Asp14	0.55	change in 4−5 ns	Phe425(C)	0.92	change in 5−6 ns
Arg18	0.63	change in 4−5 ns	Gly444(C)	0.61	change in 4−5 ns
Cys20	0.24	random	Gly446(C)	1.00	change in 5−6 ns
Asn21	0.50	random	Asp447(C)	1.00	change in 5−6 ns
Arg22	1.00	change in 4−5 ns	Met448(C)	0.63	change in 5−6 ns
Phe23	1.00	change in 5−6 ns	Thr449(C)	0.76	change in 5−6 ns
Asn24	1.00	change in 5−6 ns	Val451(C)	0.94	random
			Glu422(D)	0.72	change in 4−5 ns
	Shaker K+ channel		Asn423(D)	0.73	change in 4−5 ns
residue	fraction[a]	feature[b]	Phe425(D)	0.28	change in 4−5 ns
Phe425(A)	0.87	random	Gly444(D)	0.21	change in 4−5 ns
Thr449(A)	0.16	random	Asp447(D)	0.96	random
Ser421(B)	0.16	change in 5−6 ns	Thr449(D)	0.73	random
Glu422(B)	0.69	change in 4−5 ns	Val451(D)	0.83	random

[a] Fraction of time in which at least one contact was formed during the MD simulations. [b] Classification of change in contacts along the trajectory.

residues did not show an obvious pattern in contact formation and were grouped to a catch-all type IV (Table 3).

As listed in Table 2, five residues from κ-PVIIA and 10 residues from the *Shaker* channel formed stable contacts during the entire MD trajectory. For each of these 15 residues, the number of contacts showed only small fluctuations during the simulations. These residues should form part of the interface in the specific complex. Among the five κ-PVIIA residues, Arg2 and Lys25 suggest a possible role of electrostatic interactions, and Phe9 suggests a possible role of hydrophobic interactions. On the channel side of the interface, the selectivity-filter residues Gly444, Tyr445, and Gly446 on multiple subunits formed stable contacts through the whole simulations, showing their vital contribution to the interface. The large numbers of contacts formed by Gly446 on three of the four subunits illustrate intense interactions with κ-PVIIA (e.g., through the backbone carbonyls).

Rearrangement during 4−5 ns. Further analyses of types-II and -III residues provided details on the conformational rearrangement that occurred toward forming the specific complex. As shown in Figure 5A, Lys7 of κ-PVIIA experienced an abrupt increase of over 10 contacts around 4 ns, indicating that interactions through this residue were strengthened. An increase in contacts was also found for Leu12, while the contacts of Cys1 disappeared. Asp13, Asp14, and Arg18 appeared to undergo concerted adjustments. The contacts of Asp14 decreased sharply, all but disappearing just before 5 ns. At the same time the contacts of Asp13 and Arg18 increased sharply. Examinations of the conformations of κ-PVIIA during the simulations revealed that, initially, Asp13 and Arg18 formed a salt bridge (bottom left panel of Figure 5A). This salt bridge was later destroyed, and consequently, the two residues came into contact with the channel protein (bottom right panel of Figure 5A). During this process, the side chain of Arg22 underwent large conformational changes, and the whole toxin molecule underwent overall rotations and translations above the pore region in conjunction with the local conformational changes.

As the toxin rearranged, the contacting residues on the *Shaker* channel changed identities (Figure 6A, B). The contacts of Asn423(B), Phe425(D), and Gly444(D) decreased sharply, showing that these residues moved away from the interface. They were replaced by Glu422(B), Glu422(D), Phe425(B), Gly444(C), and Asn423(D), which had sharp increases in contacts. The movement of the negatively charged Glu422(B) and Glu422(D) to the interface was correlated with the movement of the positively charged Arg18 and Arg22 on κ-PVIIA (see below). The approach of Phe425(B) and Gly444(C) to the interface contributed to the increase in contacts formed by Lys7 on κ-PVIIA. Phe425(B) also formed hydrophobic contacts with Phe9 and Leu12 on the toxin.

Fine-Tuning during 5−6 ns. Following the significant rearrangement during 4−5 ns along the trajectory, there was additional fine-tuning during the 5−6 ns period. On the toxin side, contacts formed by Phe23 and Asn24 increased significantly (Figure 5B). On the channel side, contacts formed by Ser421(B), Asp447(B), Phe425(C), Gly446(C), Asp447(C), Met448(C), and Thr449(C) increased significantly (Figure 6C, D).

Quite a few other residues on both κ-PVIIA and the *Shaker* channel formed contacts for a significantly fraction of time (i.e., >10%) during the simulations, but the fluctuations in contacts did not show a clear pattern. As summarized in Table 3, among them, two residues (Asn5 and His11) on κ-PVIIA and eight residues [Phe425(A), Ser424(B), Lys427(B), Asn423(C), Val451-(C), Asp447(D), Thr449(D), and Val451(D)] on the *Shaker* channel spent more than 50% of the time forming contacts and could play a supporting role in the rearrangement and fine-tuning of the toxin and the channel.

Interactions in the Specific Complex. In the remaining 7.2 ns of the MD trajectory, a stable complex between κ-PVIIA and the *Shaker* channel appeared to have formed. Atomic details on the toxin−channel interactions were provided by residue−residue contact pairs collected on this portion of the trajectory (see Supporting Information). With a cutoff distance of 5 Å,

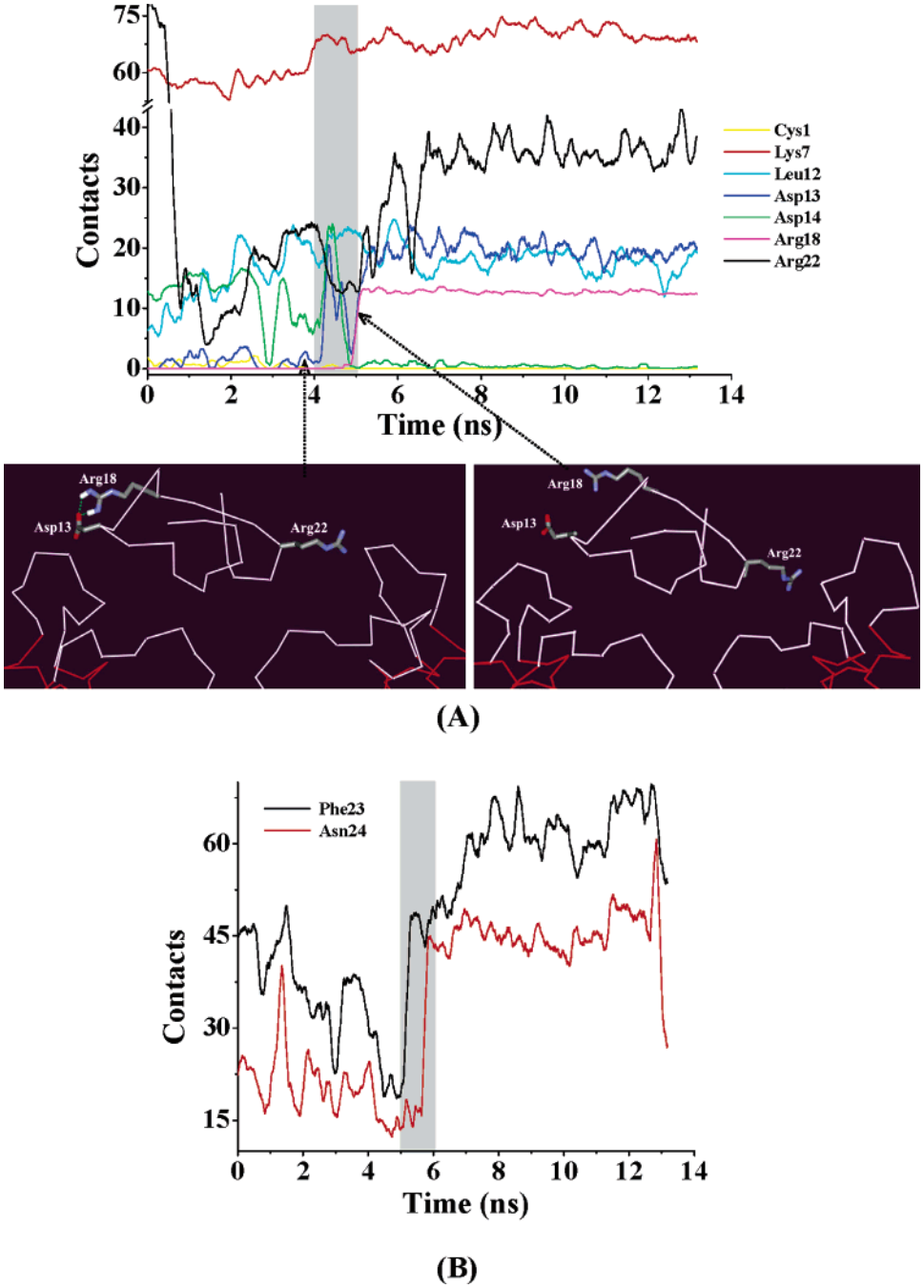

Figure 5. Changes of residue-based contacts for κ-PVIIA along the MD trajectory. (A) Type-II residues, with significant changes during 4−5 ns (shaded region). Two conformations, one at before 4 ns and one at after 5 ns, are shown to illustrate the disappearance of the intramolecular salt bridge between Asp13 and Arg18, and the significant rearrangement of the interactions between Arg22 and the loop sequence of the channel. (B) Type-III residues, with significant changes during 5−6 ns (shaded region).

49 contact pairs were found to remain formed >50% of the duration. Among these, 19 pairs had contact distances less than 3.5 Å for significant fractions of time (ranging from 38% to 100%). A dominant feature of these pairs is their complementarity, i.e., between charged residues [e.g., Arg2-Asp447(A), Arg18-Glu422(B), Arg22-Glu422(D)], between charged and polar residues [e.g., Lys7-Tyr445(A), Tyr445(B), Tyr445(C), and Tyr445(D)], between polar residues [e.g., Gln10-Asn423-(C) and Asn24-Thr449(C)], and between nonpolar residues [e.g., Phe9-Phe425(B) and Leu12-Phe425(B)].

Toxin−channel hydrogen bonds were found by the HBPLUS program,[67] using the criteria of a 3.9-Å maximum distance between donor and acceptor, a 2.5-Å maximum distance between hydrogen and acceptor, and a minimum 90° angle along donor, hydrogen, and acceptor. The numbers of hydrogen bonds formed by individual residues, averaged over the last 7.2 ns of the trajectory, are listed in Table 4. A total of ∼10 interfacial hydrogen bonds were found. Of these, four were formed between Lys7 on κ-PVIIA and the four Tyr445 residues on the *Shaker* tetramer, two each were formed between Arg18 and Glu422(B) and between Arg22 and Glu422(D), one each was formed between Gln10 and Asn423(C) and between Asn24 and

(67) McDonald, I. K.; Thornton, J. M. *J. Mol. Biol.* **1994**, *238*, 777−793.

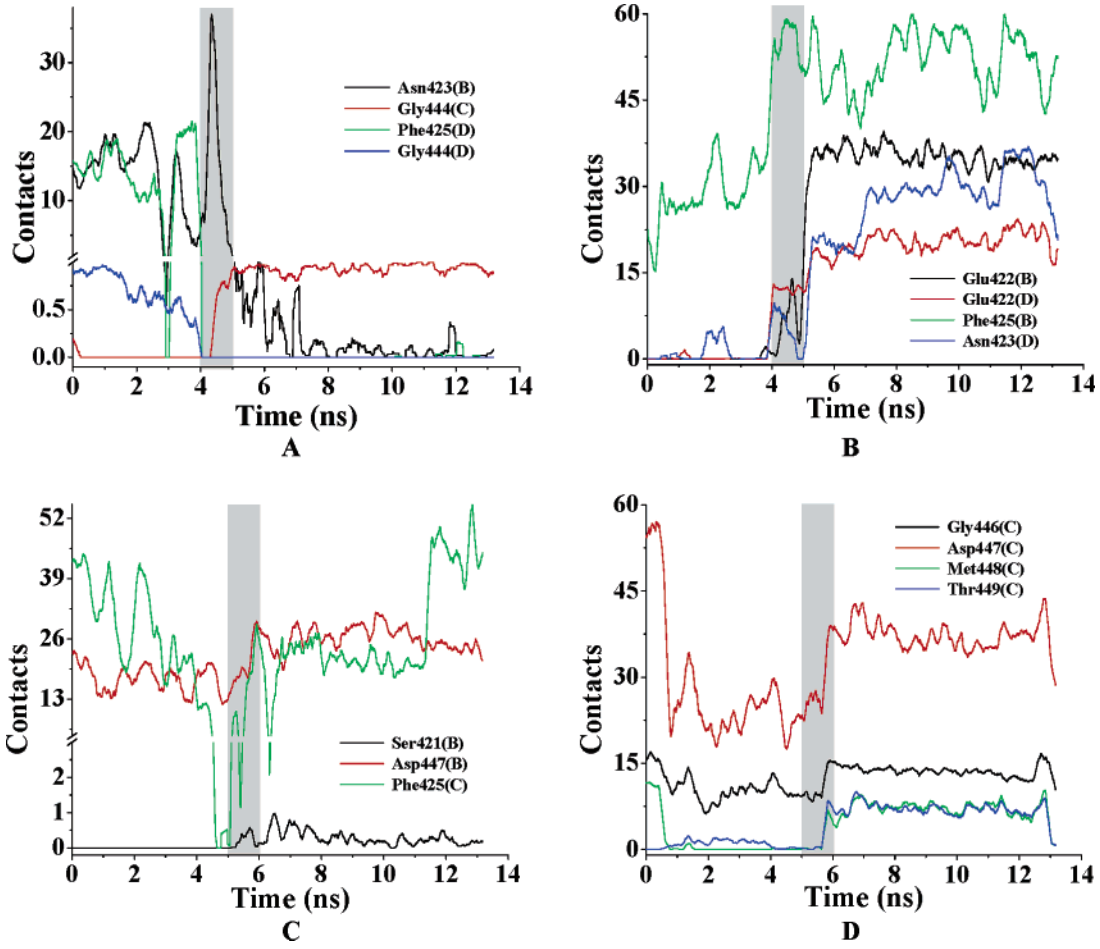

Figure 6. Changes of residue-based contacts for the *Shaker* channel along the MD trajectory. (A) and (B) Type-II residues, with significant changes during 4−5 ns (shaded region). (C) and (D) Type-III residues, with significant changes during 5−6 ns (shaded region).

Table 4. Average Number of Toxin−Channel Hydrogen Bonds Formed in the Last 7.2 ns of MD Simulations

κ-PVIIA residue	no. of hydrogen bonds	*Shaker* residues
Lys7	3.5	Tyr445(A), Tyr445(B), Tyr445(C), Tyr445(D)
Gln10	0.7	Asn423(C)
Arg18	1.9	Glu422(B)
Arg22	1.8	Glu422(D)
Asn24	1.3	Gly446(C), Thr449(C)
Lys25	0.7	Gly446(D)
Total	9.9	

Thr449(C) or the backbone carbonyl of Gly446(C), and occasionally Lys25 formed a hydrogen bond with the backbone carbonyl of Gly446(D). As noted earlier, Asp13 and Arg18 formed a salt bridge in the unbound toxin. Apparently, upon binding to the *Shaker* channel, Arg18 found a new salt-bridge partner in Glu422(B).

Missing from the list of hydrogen bonds was the interaction between toxin Arg2 and *Shaker* Asp447(A). Closer inspections of all the contacts made by these two residues showed that one or two water molecules bridged their interactions. The resulting hydrogen-bonding network suggests that Arg2 plays an important role in stabilizing the toxin−channel complex.

The nonpolar residues in the interface also appeared to make significant stabilizing contributions. In particular, the side chain of toxin Phe9 was in close contact with the side chain of *Shaker* Phe425(B) and the nonpolar portion of Lys427(B). Leu12 also formed a hydrophobic contact with Phe425(B). The side chain of Phe23 was in close contact with the nonpolar portions of a number of polar and charged residues on the channel [Asp447-(C), Glu422(D), and Asn423(D)].

A typical complex structure possessing all the interactions described above was selected from the last 7.2 ns of the trajectory. The contact distances calculated on this structure (snapshot at 7.17 ns along the trajectory) are listed in Table 5. As shown in Figure 7, in the structure κ-PVIIA and the *Shaker* channel have very good shape complementarity. Lys7 of κ-PVIIA is positioned into the vestibule of the channel, with its positively charged side chain deeply inserted into the pore. Phe9, Gln10, Phe23, Asn24, and Lys25 all fit snugly into different crevices on the channel surface. In addition, positively charged Arg2, Arg18, and Arg22 are right near negative charges on the channel. These interactions collectively provide strong stabilization to the complex.

As Table 5 and Figure 7 show, the contact residues on the toxin were dispersed throughout the entire sequence but were located on one side of the surface. On the other hand, the contact residues on the channel were from two contiguous stretches of sequence: the loop (amino acids 417−428) between the S5 and pore helices and the selectivity filter (amino acids 441−447) plus Thr449(C). The contact residues on the loop sequence were mainly from two subunits (B and D), but those on the selectivity filter involved all four subunits. The extents of conformational

Table 5. Interactions between κ-PVIIA and the *Shaker* K^+ Channel in Their Specific Complex, Calculated on the 7.17-ns Snapshot

Hydrogen Bonds				
donor		acceptor		
residue	atom	atom	residue	distance (Å)
Arg2	NH1	OH	H_2O	2.81
Arg2	NH2	OH	H_2O	2.95
Lys7	NZ	O	Tyr445(A)	2.74
Lys7	NZ	O	Tyr445(B)	2.56
Lys7	NZ	O	Tyr445(C)	2.99
Lys7	NZ	O	Tyr445(D)	3.16
Arg18	NH1	OE2	Glu422(B)	2.71
Arg18	NH2	OE1	Glu422(B)	2.79
Arg22	NH1	OE1	Glu422(D)	2.76
Arg22	NH2	OE2	Glu422(D)	2.66
Asn24	ND2	OG1	Thr449(C)	3.24
Asn24	ND2	O	Gly446(C)	3.38
Lys25	NZ	O	Gly446(D)	2.98
Asn423(C)	ND2	OE1	Gln10	2.80
H_2O	OH	OD2	Asp447(A)	2.53

Hydrophobic Contacts				
κ-PVIIA		*Shaker* K^+ channel		
residue	atom	atom	residue	distance (Å)
Phe9	CD1	CD1	Phe425(B)	3.81
Phe9	CD1	CE1	Phe425(B)	4.17
Phe9	CE2	CD	Lys427(B)	4.03
Phe9	CZ	CD	Lys427(B)	4.09
Leu12	CD2	CZ	Phe425(B)	3.81
Asp13	CB	CD	Glu422(B)	3.64
Asp13	CB	CB	Glu422(B)	3.54
Phe23	CA	CB	Asp447(C)	4.36
Phe23	CB	CB	Asp447(C)	4.70
Phe23	CD1	CB	Asp447(C)	4.76
Phe23	CE2	CB	Asn423(D)	3.83
Phe23	CZ	CB	Asn423(D)	3.78
Phe23	CZ	CD	Glu422(D)	3.85
Phe23	CZ	CB	Glu422(D)	3.81

changes made by the two stretches of sequence were also very different. Calculated on the 7.17-ns snapshot, C_α RMSDs from the initial structure were only 0.5 Å for the selectivity filter but 2.8 Å for the loop sequence. Thus, around the selectivity filter the fitting with the toxin was achieved mainly through adjustments on the latter, whereas around the loop sequence the fitting was achieved through correlated motion of both sides of the interface (see structural panels in Figure 5A).

Validation by Mutational Effects. Results for the electrostatic contributions, $\Delta\Delta G_{el}$, to the effects of 8 κ-PVIIA mutations and 16 *Shaker* mutations on the binding stability are displayed in Figure 8 (also listed in Supporting Information). These were calculated on 21 conformations sampled from the last 7.2 ns of the MD trajectory. The calculated electrostatic contributions are compared with their experimental counterparts, taken as $k_BT \ln[IC_{50}(\text{mutant})/IC_{50}(\text{wt})]$. The IC_{50} values of the mutant and wild-type toxins and channel protein were measured by Jacobsen et al.[23] Overall there is reasonable agreement between calculation and experiment on the mutational effects. The level of agreement here is generally comparable with those found in our previous studies of mutational effects on protein folding and binding stability.[11,61−63] Among the 24 mutations studied, the largest discrepancies were found for toxin mutations Arg18→Ala, Arg22→Ala, and *Shaker* mutation Glu422→Lys.

On the κ-PVIIA side, the importance of Lys7 cannot be overemphasized. In the specific complex obtained from the MD

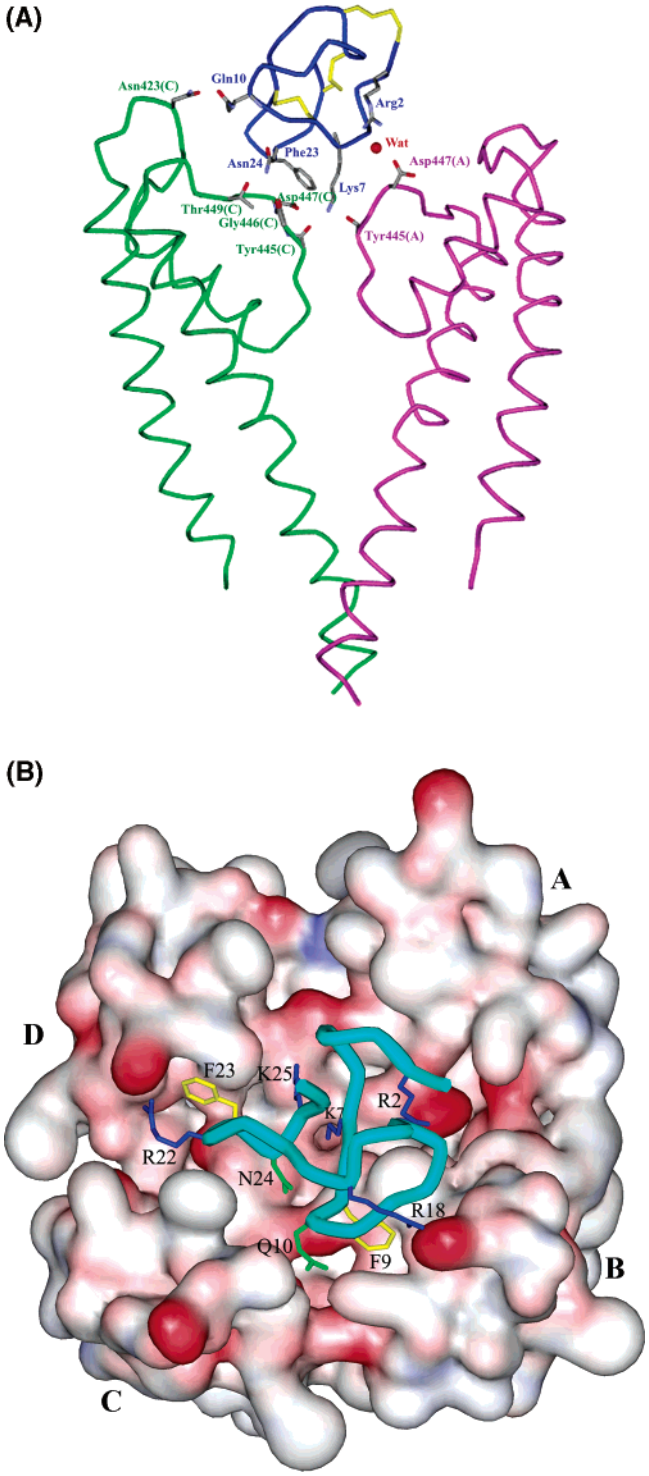

Figure 7. Structure of the 7.17-ns snapshot of the specific complex. (A) Wireframe representation showing details of intermolecular interactions. For clarity only two subunits of the *Shaker* channel protein are shown. (B) Top view of the complex, with the channel protein represented by its molecular surface color coded with the electrostatic potential (negative in red and positive in blue), with letters A−D indicating subunits. κ-PVII is shown as a cyan tube. Toxin side chains interacting with the channel are shown as sticks, with positively charged residues in blue, polar residues in green, and nonpolar residues in yellow.

simulations, its side chain forms four hydrogen bonds with Tyr445, and according to the electrostatic calculation its mutation to Ala reduces the binding stability by 5.7 kcal/mol, the largest among the eight toxin mutations studied. Jacobsen

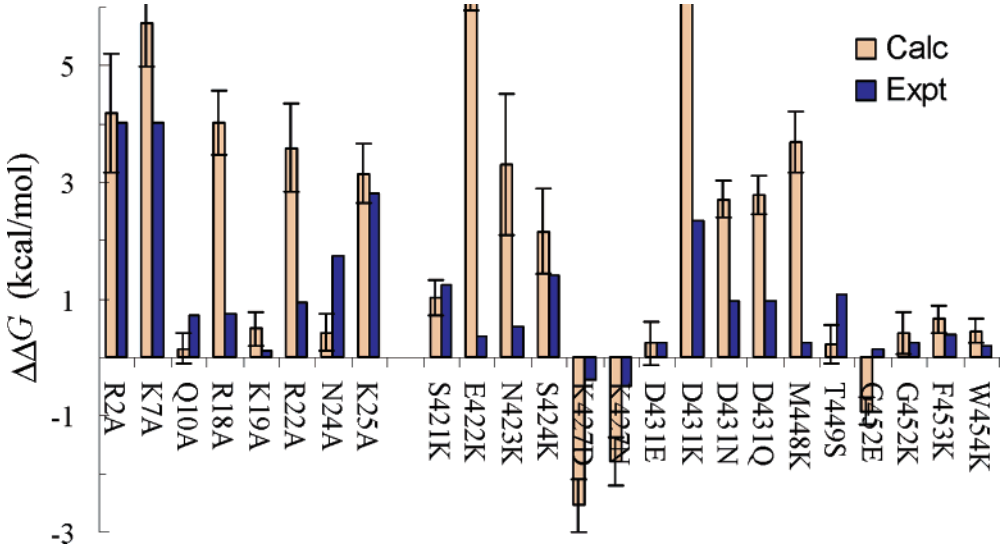

Figure 8. Comparison of calculated and experimental effects for 8 κ-PVIIA mutations and 16 *Shaker* mutations on the binding affinity. Calculated results are $\Delta\Delta G_{el}$, whereas experimental results are obtained as k_BT ln[IC_{50}(mutant)/IC_{50}(wt)] with IC_{50} values measured by Jacobsen et al.[23]

et al. observed an increase in IC_{50} from 57 to >50,000 nM, corresponding to a reduction in binding stability by over 4 kcal/mol. Therefore, the central role of Lys7 suggested by the present study appears to be in line with experiment. The large $\Delta\Delta G_{el}$ value for the Lys7→Ala is to be contrasted to the modest value of 0.5 kcal/mol for the Lys19→Ala. The latter value is expected from the positioning of Lys19 away from the interface in the MD stable complex and is in agreement with the small effect on the IC_{50} value by the mutation (from 57 to 69 nM, or a reduction of just 0.1 kcal/mol in stability).

After Lys7, the most important residues for toxin binding were Arg2 and Lys25, which are located just above the outer rim of the selectivity filter in the specific complex (Figure 7). Arg2 interacted strongly with Asp447(A) through a network of hydrogen bonds bridged by water molecules, and its mutation to Ala resulted in a $\Delta\Delta G_{el}$ of 4.2 kcal/mol. Lys25 formed a hydrogen bond with the backbone carbonyl of Gly446(D), and its mutation to Ala gave a $\Delta\Delta G_{el}$ of 3.2 kcal/mol. Both values of $\Delta\Delta G_{el}$ agree well with experimental data on IC_{50}, which correspond to losses of over 4 and 2.8 kcal/mol, respectively.

Moving away from the channel pore, Gln10→Ala and Asn24→Ala mutations were found to give much smaller values of $\Delta\Delta G_{el}$. The predicted decrease in effect on binding stability is in line with experimental data on IC_{50}, but the magnitude of the mutational effects is underestimated, perhaps because of neglect of van der Waals and hydrophobic contributions in the electrostatic calculations. Further away from the channel pore, the contributions of Arg18 and Arg22 were overestimated. It is possible that their interactions with the *Shaker* channel are not as specific and strong as in the specific complex obtained from the MD simulations. When unbound, these residues may also find alternative partners (e.g., Asp13) within κ-PVIIA for strong interactions. The effects of such rearrangements were neglected in the electrostatic calculations.

The calculated effects of the *Shaker* mutations are also in qualitative accord with experiment, although quantitatively the agreement is somewhat worse than for the toxin mutations. According to the IC_{50} measurements of Jacobsen et al., the effects of *Shaker* mutations are generally smaller than those of toxin mutations. This observation is perhaps unexpected, given that four residues in the tetrameric channel are replaced by each mutation. In agreement with experiment, residues around the start of the S6 helix (Gly452, Phe453, and Trp454) were positioned away from the interface (Figure 7), and therefore their mutations to positively (or negatively) charged residues had only a modest destabilizing (or stabilizing) effect on the binding. On the other hand, the loop between the S5 and pore helices is functionally implicated in the susceptibility to toxin binding,[20,21,24,36−39] and charge mutations of residues there (Ser421, Glu422, Asn423, Ser424, and Lys427) were found to have much stronger effects. According to the electrostatic calculations, introduction of a positive charge on Ser421, Glu422, Asn423, or Ser424 destabilized the binding, whereas neutralization or reversal of the positive charge on Lys427 led to stabilization. In comparison with the IC_{50} measurements, the magnitudes of the effects of these mutations, especially Glu422→Lys, were apparently overestimated.[68] In the specific complex, Phe425(B) formed a part of the small pocket in which κ-PVIIA Phe9 was situated (Figure 7B). The Phe425→Gly mutation, though not expected to have much electrostatic consequence, would be expected to disrupt the favorable interaction with κ-PVIIA Phe9, thus providing an explanation for the observed loss of the channel's sensitivity to κ-PVIIA binding upon the mutation.[27]

Shaker Met448 and Thr449 have been the target of a number of experimental studies on κ-PVIIA binding.[19,23,27] Koch et al.[19] and Jacobsen et al.[23] found that the mutations Met448→Lys and Thr449→Ser reduced the toxin binding stability by ~0.3 and 1.0 kcal/mol, respectively. In the specific complex obtained by our MD simulations, Thr449(C) formed a hydrogen bond with the toxin residue Asn24. In our electrostatic calculations, the Thr449→Ser mutation was found to have a $\Delta\Delta G_{el}$ value of only 0.2 kcal/mol, because in the modeled structure of the mutant Ser449(C) found an equally favorable interaction with Asn24. The Met448→Lys mutation introduced a positive charge

(68) The homology model for the channel probably was not very accurate for the loop sequence. In addition, the loop sequence underwent significant conformational adjustment in leading to the specific complex, and this adjustment was perhaps not accurately captured by the MD simulations.

to a site very close to the interface, and the electrostatic calculation gave $\Delta\Delta G_{el} = 3.7$ kcal/mol.

Among the *Shaker* mutations measured by Jacobsen et al., the charge reversal Asp431→Lys had the most destabilizing effect. The role of Asp431 in generating a field of negative electrostatic potential around the mouth of the *Shaker* pore has already been noted in the context of leading to a pre-aligned complex. After conformational adjustments, though this residue was not in direct contact with the toxin, it still could contribute significantly to the negative electrostatic potential of the channel in which the toxin is bound. When this negative charge was neutralized or reversed, large $\Delta\Delta G_{el}$ values (2.7 and 7.2 kcal/mol, respectively) were obtained.

Discussion

We have investigated the recognition and binding process of the κ-PVIIA toxin with the *Shaker* K^+ channel by complementary computational approaches. The conformational rearrangements and the specific interactions in the resulting complex provide unprecedented details on the toxin−channel binding. Though definitive test of the structure model for the toxin−channel complex must await structural probes such as X-ray diffraction, solid support for the model can be found in existing mutagenesis data. In particular, key residues identified (e.g., Lys7 and Arg2 on κ-PVIIA and Asp431 on the *Shaker* channel) are consistent with experiment. The computational approaches used and the insight gained on the binding process may also have implications for studying other peptide/protein−protein binding.

Importance of Charged Residues. A number of charged residues were found to play prominent roles in the recognition and binding of κ-PVIIA to the *Shaker* pore. The two rings of negative charges from Asp447 and Asp431 generate a field of electrostatic potential around the mouth of the *Shaker* pore, which may serve to attract the positively charged potassium ion (Figure 3). κ-PVIIA, with an abundance of positive charges, takes advantage of this field of electrostatic potential. When the toxin starts to approach the channel, it will be pre-aligned by the field of the channel for favorable electrostatic interaction. Taking advantage of charges intended for biological function appears to be a common strategy for toxins and inhibitors. For example, negative charges around the entrance to the active-center gorge of acetylcholinesterase serve to enhance the binding rate of its positively charged substrate acetylcholine.[2] Fasciculin exploits the negative charges through its own positive charges in achieving rapid binding to acetylcholinesterase.[3,4] Barnase has a number of positively charged residues around its active site that likely help it target RNA. These positive charges are used by barstar, with an excess of negative charges, for rapid binding.[5−9] The rapid inactivation of the *Shaker* channel by its N-terminal inactivation segment through occluding the cytosolic ion pore may also benefit from long-range electrostatic attraction.[10]

After the pre-alignment through long-range electrostatic attraction, charged residues continue to play important roles in the conformational adjustments and in the stability of the bound complex. Arg2 and Lys25 of the toxin may serve as important anchoring points to the channel (Table 2). The most important event in forming a specific complex is the insertion of Lys7 into the channel pore and hydrogen bonding with the four Ty445 residues. Other charged residues, such as Arg18 and Arg22 may also switch their interactions partners from intramolecular to intermolecular (Figure 5A).

The importance of charged residues in stabilizing the binding of κ-PVIIA to the *Shaker* channel is also quantitatively demonstrated by the electrostatic calculations (Figure 8). On the toxin, Lys7, through its four hydrogen bonds, and Arg2, through a hydrogen-bonding network bridged by water molecules, each contributes over 4 kcal/mol to the binding stability. Even charges at the periphery of the binding interface, particularly those of *Shaker* Lys427 and Asp431, have potential influence on the stabilization of the complex. Neutralization or reversal of the positively charged Lys427 makes a favorable contribution to the stability of the complex, whereas neutralization or reversal of the negatively charged Asp431 has the opposite effect. The great contributions of charged residues to the stability of the κ-PVIIA−*Shaker* complex found here are consistent with calculations on the barnase−barstar complex in our previous study.[11]

Significance of Conformational Adjustments. One of the difficulties in docking peptides/proteins into binding sites of their targets is the treatment of conformational flexibility of residues positioned in interfaces.[69−71] Docking algorithms frequently yield false-positive structures that are far from the native complex. The problem of induced fit, i.e., conformational adjustments in response to binding, is tackled in the present study by large-scale MD simulations.

The elaborate conformational adjustments found in the present study provide insight on induced fit. From the pre-aligned complex obtained by BD simulations, the toxin underwent overall translation and rotation with respect to the channel, while its backbone and side chains went through significant fluctuations (Figure 4). Some of the residues initially placed in the interface formed tighter interactions. These included Arg2, Lys7, Phe9, and Lys25 on κ-PVIIA. Others, such as Cys1 and Asp14, moved away from the interface (Figure 5A). At the same time yet other residues such as Phe23 and Asn24 moved in to fill the gap between the toxin and the channel that existed in the pre-aligned complex (Figure 5B). The strengthening of favorable interactions and removal of unfavorable interactions, not considered in many docking studies,[29,69−72] were found here to be very important events in leading to the specific complex.

This type of detailed information on the recognition and binding process between κ-PVIIA and the *Shaker* channel was not available from previous experimental and theoretical studies, and has been obtained here through the combination of complementary computational methods. BD and MD simulations tackled different aspects of the binding process. Validation of the resulting complex has been carried out by thorough comparison between calculated and experimental results for the effects of charged and polar residues. However, such comparison still appears to be hampered by deficiencies of the electrostatic calculations.

Mechanism of Toxin−Channel Binding. The complementary approaches of BD and MD simulations in leading to the specific toxin−channel complex also provide mechanistic insight

(69) Halperin, I.; Ma, B.; Wolfson, H.; Nussinov, R. *Proteins* **2002**, *47*, 409−443.
(70) Mendez, R.; Leplae, R.; Maria, L.; Woda, S. J. *Proteins* **2003**, *52*, 51−67.
(71) Chen, R.; Mintseris, J.; Janin, J.; Weng, Z. *Proteins* **2003**, *52*, 88−91.
(72) Moran, O. *Eur. Biophys. J.* **2001**, *30*, 528−536.

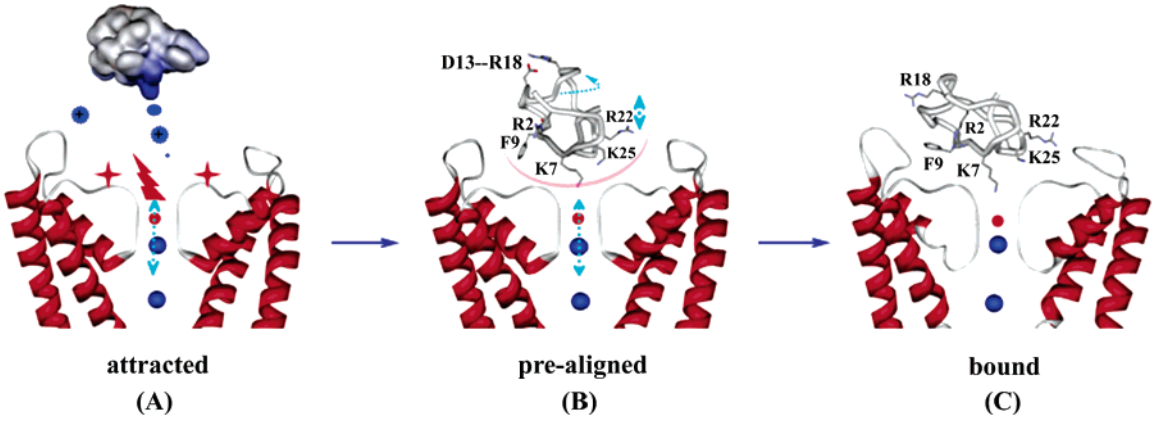

Figure 9. Mechanism of binding between κ-PVIIA and the *Shaker* channel. (A) As the toxin approaches the channel, it starts to feel the long-range electrostatic attraction of the channel. (B) The toxin comes into contact with the channel, with its orientation aligned with the channel by favorable electrostatic interactions. This pre-aligned complex can be viewed as the transition state for binding. A layer of solvent (light red arch) is still present in the interface. (C) After conformational rearrangements, the complex is stabilized. For clarity, only subunits B (left) and D (right) of the channel are shown.

(Figure 9). The BD simulations perhaps mimic the initial approach and pre-alignment, through long-range electrostatic interactions, of the toxin toward the channel. With Arg2, Lys7, and Lys25 anchored on the channel, the initial complex is formed (Figure 9B). This initial complex is unstable and may either become separated or become tightly bound, and thus can be ascribed as the transition state.[7,8] The ensuing conformational adjustments that lead to the specific complex are mimicked by the MD simulations. During the process, the space in the interface becomes completely filled up, numerous favorably interactions are formed, and shape complementarity is reached (Figure 9C). This proposed binding mechanism appears to be a general one.

Implications for other Toxin−Channel Interactions. Toxins have been used as an important tool for characterizing structure and function of voltage-gated potassium channels, because of their unique blockage of K^+ currents and other physiological functions.[14−20,23,27,29,43,48,49] κ-PVIIA shares surface features with other toxins with enriched positively charged residues,[14,15] while the *Shaker* channel is a well-known representative of Kv channels.[20−31] The detailed information on the recognition and binding process of this prototypical toxin−channel system obtained in the present study should help elucidate toxin−channel interactions in general.

The binding mode of κ-PVIIA appears similar to the way in which agitoxin binds to the *Shaker* pore, in that a positively charged side chain of the toxin is deeply inserted into the central pore. The latter was revealed by experimental agitoxin footprinting[20,21] and simulations on agitoxin−*Shaker* binding.[29] Similar involvement of *Shaker* Ser424, Phe425, Asp447, and Met448 in agitoxin binding suggests that these residues are commonly recognized by different toxins. Besides κ-PVIIA and agitoxin, other toxins such as maurotoxin (MTX), charybdotoxin (CTX), and the short peptide TC1 also block the *Shaker* channel. Among these toxins, κ-PVIIA binds to *Shaker* with the highest binding affinity. There does not appear to be obvious relationship between binding affinities and structural folds of toxins.[20,27,43,49] Rather, phylogenetic tree analysis indicates that the physiological actions, specificity, and affinities of a wide variety of toxins depend on the amino acids situated on the surfaces.[43] The present study demonstrates that these surface residues as well as the loop sequence of the channel protein undergo significant conformational rearrangements upon binding. These rearrangements are likely to be important for binding affinity and specificity but are difficult to predict without MD simulations. A toxin may also affect functionally important internal dynamics of the target protein.[73]

While many toxins can bind to a single Kv channel, a single toxin can also block many Kv channels. In particular, both MTX and CTX can block *Shaker*, Kv1.1, Kv1.2, Kv1.3, among others.[18−21,23,27,29,49] Sequence−function analysis on a family of Kv channels reveals that the selectivity filter and the pore helix are highly conserved.[24] Available X-ray structures of Kv channels also show strong structural similarity.[32−35,40−42] The sequence and structure conservation may partly explain the apparent cross-interactions of toxins and Kv channels. Further understanding of toxin binding affinity and specificity may be achieved by applying the computational approaches of the present study on the binding of several different toxins with one Kv channel, or the binding of one toxin with several Kv channels. Interplay with physiological experiments will be valuable in gaining additional insights on the structure and function of Kv channel−toxin interactions.

Conclusion

The present work has yielded unprecedented information on the recognition and binding of κ-PVIIA to *Shaker* K^+ channel. Through BD simulations, it was found that the recognition between toxin and channel is greatly facilitated by long-range electrostatic attraction. According to electrostatic interaction energies calculated on configurations from BD simulations, the binding mode with Lys7 of κ-PVIIA occluding the pore of the *Shaker* channel was selected. MD simulations revealed an intricate process of induced fit lasting a period of ∼6 ns. Especially in a time window of 2 ns, favorable contacts were formed or strengthened, and unfavorable contacts were eliminated, leading to a specific complex. This complex was stabilized by numerous favorable electrostatic and hydrophobic interactions. In particular, the side chain of κ-PVIIA Lys7 inserted deeply into the central pore, forming four hydrogen bonds with *Shaker* Tyr445. Electrostatic calculations of mutational effects on the specific complex correlated reasonably well with experimental data on IC_{50} values. A binding mechanism,

(73) Bui, J. M.; Tai, K.; McCammon, J. A. *J. Am. Chem. Soc.* **2004**, *126*, 7198−7205.

consisting of pre-alignment through long-range electrostatic attraction and induced fit through local conformational rearrangements, is proposed. The detailed information on the recognition and binding process of a prototypical toxin−channel system should help elucidate peptide/protein−protein interactions in general.

Acknowledgment. This work was supported in part by NIH Grant GM58187. We thank J. Andrew McCammon and Jung-Hsin Lin for kindly providing the parameters and coordinates of POPC molecules.

Supporting Information Available: A table listing residue−residue contact pairs in the last 7.2 ns of MD simulations and a table listing effects of mutations on binding affinity. This material is available free of charge via the Internet at http://pubs.acs.org.

JA042641Q